Journal of Applied Mathematics and Physics, 2021, 9, 1837-1852
https://www.scirp.org/journal/jamp
ISSN Online: 2327-4379
ISSN Print: 2327-4352

Facile Preparation of Novel Manganese Dioxide Modified Nanofiber and Its Uranium Adsorption Performance

Wuqing Tao[1,2], Riwen Lv[2], Qinqin Tao[2*]

[1]Department of Radiochemisty, China Institute of Atomic Energy, Beijing, China
[2]State Key Laboratory of Nuclear Resources and Environment, East China University of Technology, Nanchang, China
Email: *taoqinqin@ecut.edu.cn

How to cite this paper: Tao, W.Q., Lv, R.W. and Tao, Q.Q. (2021) Facile Preparation of Novel Manganese Dioxide Modified Nanofiber and Its Uranium Adsorption Performance. *Journal of Applied Mathematics and Physics*, **9**, 1837-1852.
https://doi.org/10.4236/jamp.2021.97118

Received: May 11, 2021
Accepted: July 27, 2021
Published: July 30, 2021

Abstract

In this study a novel manganese dioxide modified nanofiber was facile prepared using the electrospinning technique. The as-prepared manganese dioxide/poly(vinyl alcohol)/poly (acrylic acid) (briefly as MnO_2-PVA/PAA) was firstly characterized by SEM, FT-IR, XRD, stress-strain test and secondly tested as an adsorbent to remove uranium from aqueous solution. Effect of pH, ionic strength, initial uranium concentration, mixing time, temperature on the adsorption, reusability and adsorption mechanism were illustrated. The theoretical adsorption amount of MnO_2-PVA/PAA calculated as 398.85 mg/g was competitive compared with the reported values. The study proved MnO_2-PVA/PAA is promising in the uranium removal from aqueous medium.

Keywords

Uranium, Manganese Dioxide, Nanofiber, Electrospin

1. Introduction

Global fossil fuels such as coal, petroleum and natural gas are being intensively consumed and expectedly depleted within two hundred years in terms of currently annual consumption [1]. Nuclear energy is an extremely important candidate owning to high energy density (3.9×10^6 MJ/Kg uranium) [2] and zero greenhouse gas emissions [3]. Nevertheless, there is a tricky problem associating with nuclear energy. Uranium is an element of non-degradable nature, strong fluidity and long-lasting pollution of chemical and biological toxicity. By aqueous organisms uranium can migrate with the food chain readily, finally into

human body. Once over the limited range many fatal and irreversible injuries occur in lungs, kidneys or other organisms. The World Health Organization prescribes uranium limit as 14.4 μg/L [4]. Overall remediation of waters contaminated by uranium is of great significance.

At present many remediation approaches includes chemical precipitation [5], solvent extraction [6], ion exchange [7], particle flotation [8], membrane separation [9], catalytic [10] and adsorption [11] [12], in which the adsorption attains more attention due to high feasibility, low energy cost and less second waste. Besides adsorption craft parameters the adsorbent plays a key role.

Metal oxide is explored as an effective kind of adsorbent for waste water remedy. Manganese dioxide (MnO_2) presents excellent potentiality in this respect owing to acidity stability, negatively charged surface, low cost and high affinity [13]. The challenges in utilization of manganese dioxide as an adsorbent are as following: 1) Uranium uptakes of the raw manganese dioxide were demonstrated as commonly less than 60 mg/g [14]; 2) The fine particle size and aggregation of manganese dioxide lead to the difficulty in solid-liquid separation as well as the low efficiency in removal of uranium. It is such reason that many modification of manganese dioxide were conducted. For example, Zhu *et al.* [15] used poly(N-hydroxymethylacrylamide/2-hydroxyethylacrylate)hydrogel immobilized manganese dioxide for removal of Pb^{2+}, Cu^{2+}, Cd^{2+} and Ni^{2+}. Kim *et al.* [16] fabricated magnetic manganese dioxide nanocomposites (Fe_3O_4/MnO_2), which could be recovered by an external magnet.

Electrospinning is one of the most compatible techniques to produce continuous nanofibers of inorganic, organic, metals and composites [17]. The as-produced nanofibers often with large specific surface area and abundant porosity are promising in the fields of catalysis [18], batteries [19], medicine [20] and separation [21] [22]. To separate metal ions many electrospinning nanofibers were reported, for example, polyacrylonitrile/SiO_2 for Th^{4+}, U^{6+}, Cd^{2+} and Ni^{2+} [23], polyvinylpyrrolidone/CeO_2/(3-mercaptopropyl)trimethoxysilane for Pb^{2+} and Cu^{2+} [24], poly(vinyl alcohol)/tetraethoxysilane/(3-aminopropyl) triethoxysilane for Cd^{2+} [25], poly(vinyl alcohol)/titanium oxide/zinc oxide for Th^{4+} [26], polyvinylpyrrolidone/iron acetylacetonate for Hg^{2+} [27], poly(vinyl alcohol)/titanium oxide for Th^{4+} and uranyl [28], chitosan/multi-walled carbon nanotubes for Cr^{6+} [29], chitosan/hydroxyapatite for Pb^{2+}, Co^{2+} and Ni^{2+} [30].

In the study of MnO_2-PVA/PAA nanofiber was prepared by electrospinning and further *in-situ* coating. Advantages of the consequent MnO_2-PVA/PAA are as following: 1) high availability; 2) better uranium separation performance including high uranium uptake capacity, reusability and mechanical strength. MnO_2-PVA/PAA was tested for uranium separation effectivity at different pH, ionic strength, adsorption time, initial uranium concentration and temperature. The kinetics, isotherms, thermodynamics, reusability and membrane performance were discussed. The results herein demonstrated the high potential of MnO_2-PVA/PAA as a candidate in membrane separation for uranium.

2. Experimental Section

2.1. Materials and Instruments

All chemicals of reagent-grade purity were attained from commercial companies and directly utilized as received. The surface morphology of electrospinning nanofiber was measured by SEM (Nova Nano 450, Netherlands FEI Company). Chemical groups in nanofiber were observed by FT-IR (Nicolet 380, Thermo Nicolet Corporation). The crystal structure was determined by XRD (D8. Advance, Shuyun instruments (Shanghai) Co., Ltd). XPS measurement was performed with Escalab 250 Xi (Thermo Fisher). The hydrophily was analyzed by measuring contact angle (JC2000C1, Shanghai Zhongchen Digital Co., Ltd.). The mechanical property was measured using Universal mechanical testing machine (WDT-5, Shenzhen Kaiqiangli Experimental Instrument Company).

2.2. Preparation of PVA/PAA and MnO_2-PVA/PAA Nanofiber

The solution composed of 1.6 g poly (vinyl alcohol) and 10 mL deionized water was magnetically stirred to homogeneous phase at 85˚C, followed by addition of 0.3 g poly (acrylic acid). After cooling down to room temperature the resultant solution stirred for well-mix was stored as the electrospinning precursor solution.

The electrospinning operation for PVA/PAA nanofiber was described as the following. The above precursor solution was transferred in a syringe equipped with a stainless-steel needle of 22 G that serving as the anode. A rotation drum connected with the cathode was used as a collector. The anode-cathode voltage and distance were set as 23.5 kV and 15 cm, respectively. The flow rate was fixed as 0.5 mL/h. The collected nanofiber was thermo-treated for 3 h for cross-linking esterification reaction between PVA and PAA. The final mat was poly(vinyl alcohol)/poly(acrylic acid) nanofiber briefly as PVA/PAA.

In-situ coating of MnO_2 onto PVA/PAA was completed via a redox chemical reaction. Specifically, the mixture containing 1.0 g PVA/PAA and 100 mL potassium permanganate solution (2.0 g/L) was agitated for 2 h at 35˚C at pH = 2.0, followed by dropwise addition of 5.0 mL absolute ethanol. The resultant solution was continuously agitated for 30 min until clarification. The nanofiber was taken out from the solution, washed with deionized water for three times, and dried at 85˚C for 5 h. The as-prepared product was named as MnO_2-PVA/PAA nanofiber.

2.3. Uranium Adsorption Performance Test

All batchwise experiments were conducted by controlling MnO_2-PVA/PAA mass as 10 mg and solution volume as 50 mL. The solution pH was kept at 6.0 except the study on pH influence where pH was from 2.5 to 6.0 with interval value of 0.5. The $NaClO_4$ concentration was zero except the study on effect of ionic strength, in which $NaClO_4$ concentration ranged from 0.1 mol/L to 0.6 mol/L. The uranium concentration in feed solution was fixed at 50 mg/L except

the isotherms study. The duration was set as 2 h except the kinetics research where it varied from 5 min to 150 min. The environmental temperature was controlled at 298.15 K except in thermodynamics experiment, in which it was in the range of 288.15 K to 318.15 K with an interval of 5 K. After adsorption, the nanofiber was taken out and the residue uranium concentration in solution was detected with the standard arsenazo III method. The uranium uptake amount (q_e (mg/g)) was calculated out using Equation (1):

$$q_e = \frac{([UO_2^{2+}]_0 - [UO_2^{2+}]_e)V}{m} \quad (1)$$

where $[UO_2^{2+}]_0$ is uranium concentration in the feed solution (mg/L); $[UO_2^{2+}]_e$ is uranium concentration (mg/L) before solid-liquid separation; V (L) is the volume of uranium-containing feed solution; m (g) is the mass of MnO_2-PVA/PAA or PVA/PAA.

The strip experiment followed the adsorption experiment were carried out by washing the spent nanofiber with eluate solution (50 mL, 1.0 mol/L) such as HCl, H_2SO_4, HNO_3, Na_2CO_3, EDTA. The strip efficiency was figured out using Equation (2):

$$D\% = \frac{C_D \times V_D}{q_e} \times 100 \quad (2)$$

where C_D is uranium concentration in eluate (mg/L). V_D is the volume of the collected eluate (L). q_e is the uptake amount before strip (mg/g).

For the recycling experiments, the recovered MnO_2-PVA/PAA or PVA/PAA regenerated using HCl (1.0 mol/L) was applied to adsorb uranium repeatedly.

3. Results and Discussion

3.1. Characterization

The microscopic morphologies of PVA/PAA and MnO_2-PVA/PAA are shown in **Figure 1(a)**, **Figure 1(b)**. One can see that both nanofibers were non-directional homogeneous fiber beams without beads. The average diameter were 270 nm for PVA/PAA and 320 nm for MnO_2-PVA/PAA. The particles on MnO_2-PVA/PAA surface were MnO_2. The FT-IR spectrum shown in **Figure 1(c)** displayed the characteristic bands of PVA/PAA at 3340 cm^{-1}, 2942 cm^{-1}, 1710 cm^{-1}, 1090 cm^{-1} and 850 cm^{-1} were resulted from vibrations of hydroxyl, C-H asymmetric, C=O in carboxyl and ester groups, C-O-C from the crosslinking reaction of PVA and PAA stretching and C-H bending. The FT-IR spectrum of MnO_2-PVA/PAA retained the characteristic bands of PVA/PAA and meanwhile highlighted characteristic bands of MnO_2 at 1370 cm^{-1} and 559 cm^{-1} assigned as stretching vibration of Mn-OH and Mn-O. XRD patterns shown in **Figure 1(d)** indicated MnO_2 indeed existed in MnO_2-PVA/PAA according to PDF#44-0092. The stress-strain curve of PVA/PAA and MnO_2-PVA/PAA are shown in **Figure 1(e)**, **Figure 1(f)**. As can be seen, as the immersion duration increased, stress-strain of PVA/PAA and MnO_2-PVA/PAA decreased. The reason was attributed to the corrosion from the aqueous solution.

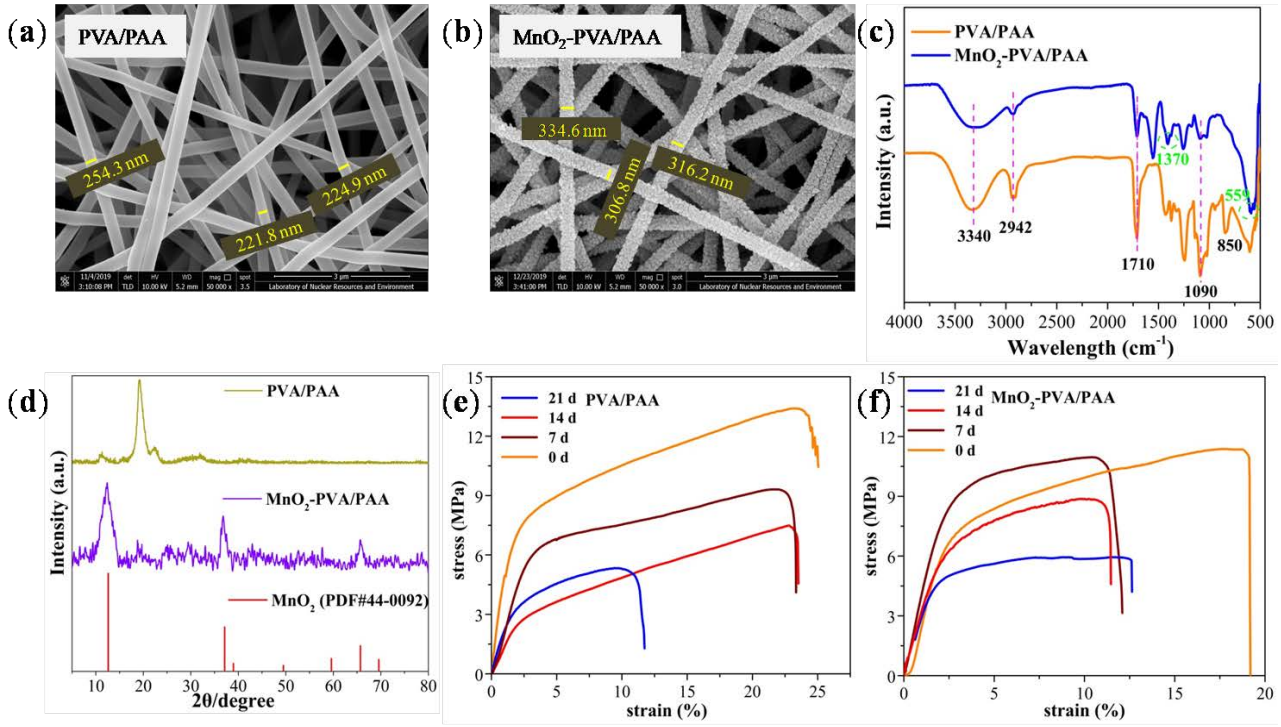

Figure 1. SEM images of (a) PVA/PAA, (b) MnO_2-PVA/PAA; (c) FT-IR spectra of PVA/PAA and MnO_2-PVA/PAA; (d) XRD patterns of PVA/PAA and MnO_2-PVA/PAA; Stress–strain curves of PVA/PAA (e) and MnO_2-PVA/PAA (f).

3.2. Effect of pH and Ionic Strength on Uranium Adsorption

The uranium uptake amount varying with pH is shown in **Figure 2(a)**. It can be seen that pH increasing from 2.5 to 6.0 was beneficial for uranium adsorption. The further increase in pH would count against the adsorption. The explanation for the results was as following. Firstly positive charged species such as UO_2^{2+}, $UO_2(OH)^+$, $(UO_2)_2(OH)_2^{2+}$, $(UO_2)_3(OH)_4^{2+}$, $(UO_2)_3(OH)_5^+$ and $(UO_2)_4(OH)_7^+$ were dominant at pH < 6.0, which showed high affinity toward both nanofibers. Secondly more hydrogen ion at lower pH could weaken the adsorption ability through protonating the nanofibers and occupying the adsorption sites.

Effect of $NaClO_4$ concentration in the range of 0 mol/L to 0.6 mol/L on the adsorption is conducted to illustrate the ionic strength influence and the result is shown in **Figure 2(b)**. It can be seen that as $NaClO_4$ concentration increased, the uranium adsorption on both fibers varied slightly. The result proved that the adsorption of uranium on both fibers werein the way of the inner-sphere surface complex [31]. The finding agreed with other uranium adsorption phenomenon reported in the literature [32].

3.3. Adsorption Isotherms

Effect of initial uranium concentration on the adsorption onto PVA/PAA and MnO_2-PVA/PAA are shown in **Figure 3**. It can be seen that q_e increased with the increase in C_e. The reasonable explanation was that higher concentration gradient promoted the utilization in adsorption sites. To explain the adsorption

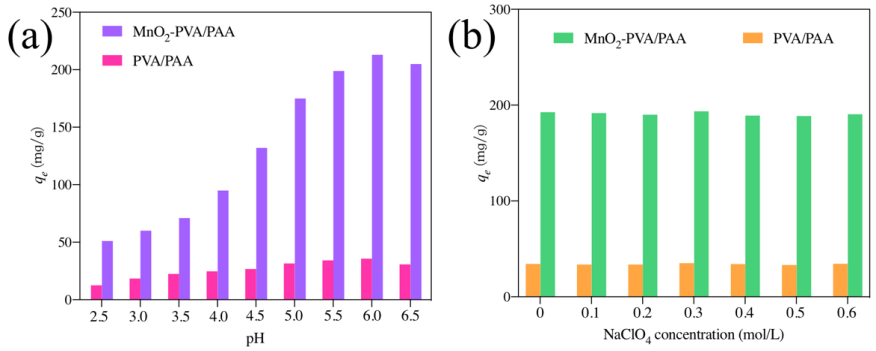

Figure 2. (a) Effect of pH on uranium adsorption onto PVA/PAA and MnO_2-PVA/PAA (C_0 = 50 mg/L, V = 50 mL, m = 10 mg, mixing time = 2 h, T = 298.15 K); (b) Effect of ionic strength on uranium adsorption (C_0 = 50 mg/L, m = 10 mg, V = 50 mL, pH = 6.0, mixing time = 2 h, T = 298.15 K).

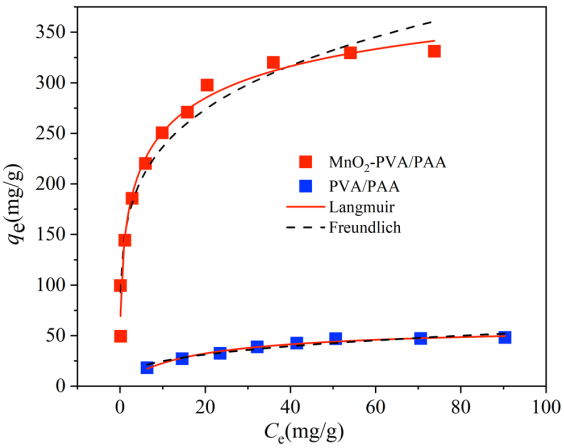

Figure 3. Effect of initial U (VI) concentration on adsorption capacity. (m = 10 mg, V = 50 mL, pH = 6.0, mixing time = 2 h, T = 298.15 K).

mechanism, the data were further analyzed by fitting Langmuir and Freundlich isotherm models.

The Langmuir model is associated with identical active sites and surface coverage in the way of single layer. Its mathematical description is shown in Equation (3):

$$q_e = \frac{K_L q_m C_e}{1 + K_L C_e} \tag{3}$$

where C_e (mg/L) and q_e (mg/g) are uranium concentration and uptake amount at equilibrium state; q_{max} (mg/g) is the theoretically saturation uptake amount; b (L/mol) is the Langmuir constant.

The Freundlich model fits well with the adsorption on hetergeneous adsorption sites. Its empirically mathematical equation is presented as Equation (4).

$$q_e = K_F C_e^{1/n} \tag{4}$$

where n (mg/g) and K_F ($mol^{1-n} \cdot L^n/g$) are used to measure adsorption intensity and uptake amount, respectively.

As can be seen from **Table 1**, R^2 values of the Langmuir model were closer to 1.0 than the values of Freundlich. It could be concluded that the adsorption processes were in agreement with the assumption of Langmuir model. Both adsorption processes took the monolayer way. The modification using MnO_2 significantly improved the adsorption amount from 58.51 mg/g to 398.85 mg/g.

The theoretical q_e of MnO_2-PVA/PAA achieved to 398.85 mg/g, a very competitive value compared with other adsorbent materials (shown in **Table 2**). The competitive q_e of MnO_2-PVA/PAA might originated from high disperse of MnO_2 on PVA/PAA surface proved in **Figure 1(b)**.

3.4. Adsorption Kinetics

Figure 4 shows the effect of mixing time on adsorption of U (VI) with PVA/PAA and MnO_2-PVA/PAA. It can be found that the variation in q_e presented three phases including: 1) the rapid boost stage within 0 - 20 min resulted from abundant unoccupied sites; 2) the slow increase stage between 20 min - 120 min due to insufficient adsorption sites; 3) the steady stage after 120 min attributed to the dynamic state equilibrium.

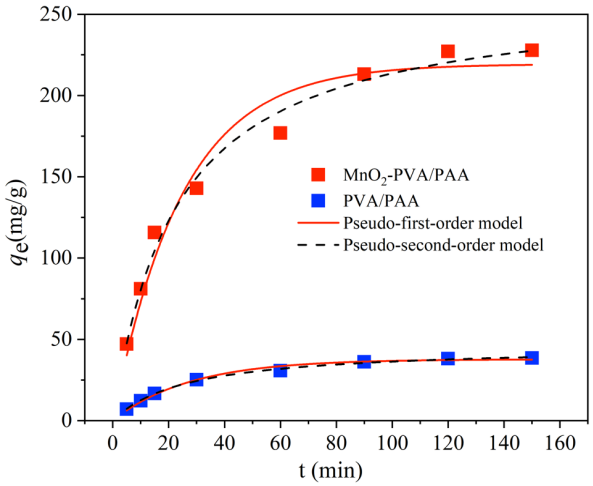

Figure 4. Effect of mixing time on adsorption capacity. (C_0 = 50 mg/L, m = 10 mg, V = 50 mL, pH = 6.0, T = 298.15 K).

Table 1. The parameters of Langmuir and Freundlich isotherm models for uranium adsorption on PVA/PAA and MnO_2-PVA/PAA.

Parameters	MnO_2-PVA/PAA	PVA/PAA
	Langmuir	
q_{max} (mg/g)	398.85	58.51
b (L/mol)	0.004	0.032
R^2	0.995	0.983
	Freundlich	
K_F ($mol^{1-n} \cdot L^n/g$)	23.01	8.91
1/n	0.46	0.38
R^2	0.935	0.919

Table 2. The maximal adsorption capacity of various sorbents for uranium.

Adsorbents	Experimental parameters	Qmax (mg/g)	Reference
HMO	pH = 5.0, T = 298 K	57.6	[33]
SBA-15	pH = 6.0, T = 298 K	203	[34]
NIMS-4	pH = 6.0, T = 298 K	79.2	[35]
CNFs	pH = 4.5, T = 298 K	125	[36]
U-PASS	pH = 5.0, T = 303 K	147.8	[37]
DSHM-DAMN	pH = 8.0, T = 298 K	601	[38]
HGly	pH = 5.0, T = 293 K	186.5	[39]
PVP/chitosan	pH = 5.9, T = 298 K	167	[40]
PAF	pH = 5.0, T = 303 K	115.31	[41]
Magnetic biochar	pH = 4.0, T = 318 K	52.63	[42]
Polypyrrole	pH = 5.0, T = 298 K	87.72	[43]
P(AO)-g-CTS/BT	pH = 8.0, T = 298 K	49.09	[44]
Fe-Al LDHs	pH = 6.0, T = 298 K	99.01	[45]
MnO_2-PVA/PAA	pH = 6.0, T = 298 K	398.85	this study

To illuminate kinetics process in detail, two frequently used models, pseudo-first-order Equation (5) and pseudo-second-order Equation (6) kinetics equations, were adopted to fit the data.

$$q_t = q_e(1-e^{-k_1 t}) \tag{5}$$

$$q_t = \frac{q_e^2 k_2 t}{1+q_e k_2 t} \tag{6}$$

where q_t (mg·g^{-1}) and q_e (mg·g^{-1}) are the uptake amount at time t (min) and equilibrium, respectively; k_1 (min^{-1}) and k_2 (g·mg^{-1}·min^{-1}) represent adsorption rate constants, respectively.

The fitting values are listed in **Table 3**. It can be clearly seen that: 1) the correlation coefficients values derived from the pseudo-second-order kinetics (0.997 for PVA/PAA and 0.987 for MnO_2-PVA/PAA) were closer to 1.0 than the pseudo-first-order kinetics (0.987 for PVA/PAA and 0.957 for MnO_2-PVA/PAA); 2) the experimentally maximal uptake amounts (38.52 mg/g for PVA/PAA and 227.87 mg/g for MnO_2-PVA/PAA) were more approximate to the theoretical values (42.16 mg/g for PVA/PAA and 242.56 mg/g for MnO_2-PVA/PAA) from the pseudo-second-order kinetics rather than the theoretical values (33.04 mg/g for PVA/PAA and 193.29 mg/g for MnO_2-PVA/PAA) from the pseudo-first-order kinetics. The consequent parameters proved both adsorption processes were coincide with the assumption of the pseudo-second-order kinetics. The results indicated both adsorption processes are mainly chemical.

3.5. Adsorption Thermodynamics

The effect of temperature (288.15 K - 318.15 K) on the adsorption of uranium

Table 3. The calculated parameters of pseudo-first-order and pseudo-second-order models fitting the adsorption of uranium on PVA/PAA and MnO_2-PVA/PAA.

Materials	$q_{e,exp}$ (mg/g)	Pseudo-first-order model			Pseudo-second-order model		
		$q_{e,cal}$ (mg/g)	k_1	R^2	$q_{e,cal}$ (mg/g)	k_2	R^2
PVA/PAA	38.52	33.04	0.0364	0.987	42.16	8.24×10^{-4}	0.997
MnO_2-PVA/PAA	227.87	193.29	0.0405	0.957	242.56	1.69×10^{-4}	0.987

with PVA/PAA and MnO_2-PVA/PAA were studied. The results are shown in **Figure 5(a)**. It can be seen that both q_e slightly increased with the increase in temperature. It is revealed that a higher temperature favored the adsorption.

To study the thermodynamic nature of the adsorption, the thermodynamic parameters such as ΔH° and ΔS° were calculated out by Equation (7) from the slope and intercept of the linear plot between $\ln K_d$ *vs.* $1/T$. The change in Gibbs free energy ΔG° values was acquired using Equation (8).

$$\ln K_d = \frac{\Delta S^\circ}{R} - \frac{\Delta H^\circ}{RT} \tag{7}$$

$$\Delta G^\circ = \Delta H^\circ - T\Delta S^\circ \tag{8}$$

where K_d (mL·g^{-1}) is the distribution coefficient at the equilibrium state; R (8.314 J·K^{-1}·mol^{-1}) is the ideal gas constant; T (K) is thermodynamic Kelvin temperature.

$\ln K_d$ as a function of $1/T$ is shown in **Figure 5(b)**. The obtained values are listed in **Table 4**. ΔH° and ΔS° of positivity indicated both adsorption were endothermic processes with entropy increase. The negative ΔG° values proved that both adsorptions were spontaneous. A higher temperature leading to a higher absolute value of ΔG° illustrated that increasing temperature promoted the adsorption process. In addition, the absolute value of ΔG° for MnO_2-PVA/PAA was greater than that of PVA/PAA, indicating that MnO_2-PVA/PAA was more likeable for U(VI) than PVA/PAA.

3.6. Desorption, Reusability

The reusability is an important indicator for the practical application of a material. The desorption behavior of PVA/PAA and MnO_2-PVA/PAA were studied using stripping reagents such as HCl, H_2SO_4, HNO_3, Na_2CO_3 and ethylenediaminetetraacetic acid (EDTA) of 1.0 mol·L^{-1}. The desorption rate D% are shown in **Figure 6(a)**. It is found that HCl solution had the most efficient strip ability. The reason maybe that Cl^- with stronger polarity combined with UO_2^{2+} to form $UO_2Cl_3^-$ readily. HCl solution was thus used for the next adsorption-desorption cycle experiments.

The adsorption-desorption cycle experiments was conducted to assess the reusability of MnO_2-PVA/PAA. HCl solution of 1.0 mol·L^{-1} was used as the desorption reagent. The result is shown in **Figure 6(b)**. It can be seen that the uptake amount (q_e) decreased as the cycle time increased. The decrease was resulted from the decrease in effective adsorption sites. Firstly HCl solution could

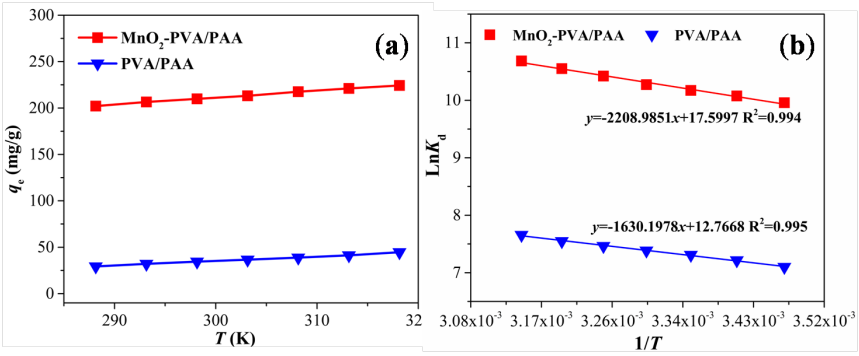

Figure 5. (a) Effect of temperature on adsorption capacity; (b) linear plots of lnK_d *vs.* 1/T (C_0 = 50 mg/L, m = 10 mg, V = 50 mL, pH = 6.0, mixing time = 2 h).

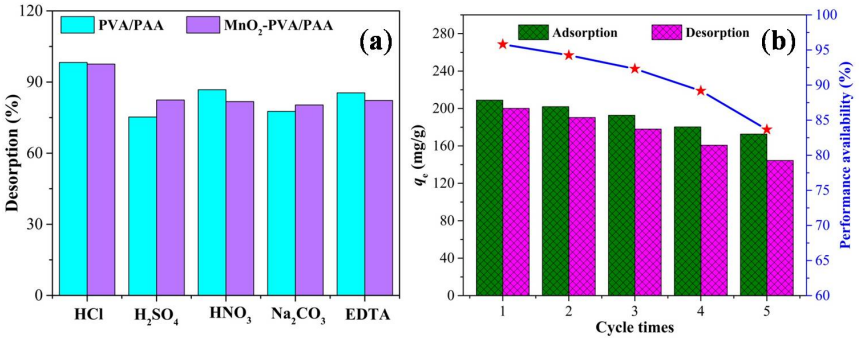

Figure 6. (a) Desorption efficiency of many eluents; (b) Reusing performance of MnO_2-PVA/PAA. (C_0 = 50 mg/L, m = 10 mg, pH = 6.0, mixing time = 2 h, T = 298.15 K.)

Table 4. Thermodynamic parameters of adsorption of uranium onto PVA/PAA and MnO_2-PVA/PAA.

Parameters	Temperature (K)	PVA/PAA	MnO_2-PVA/PAA
ΔH° (kJ·mol^{-1})	-	13.55	18.37
ΔS° (J·K^{-1}·mol^{-1})	-	106.04	146.32
	288.15	−17.03	−23.79
	293.15	−17.56	−24.52
	298.15	−18.10	−25.26
ΔG° (kJ·mol^{-1})	303.15	−18.63	−25.99
	308.15	−19.16	−26.72
	313.15	−19.69	−27.45
	318.15	−20.22	−28.18

not completely desorb all the uranium adsorbed on MnO_2-PVA/PAA; Secondly the adsorption in the chemical way of the inner-sphere surface complex was not fully reversible. Even so q_e decreased from the initial 208.87 mg/g to the final 172.65 mg/g after five cycles.

3.7. Mechanism Explored with XPS

To explore the interaction of uranyl with MnO_2-PVA/PAA in the molecular lev-

el, XPS was used to reveal the binding energy of MnO_2-PVA/PAA and MnO_2-PVA/PAA-U(VI). C, O and Mn, the major composition of MnO_2-PVA/PAA, were verified by C 1s, O 1s and Mn 2p peaks in **Figure 7**. Due to the characteristic doublet of U 4f (shown in **Figure 7(a)**, **Figure 7(e)**), it was no doubt that uranium had been adsorbed on the near-surface of MnO_2-PVA/PAA. As can be seen in **Figure 7(e)**, U 4f was splitted into U $4f_{5/2}$ and U $4f_{7/2}$, of which the former corresponded to U-O in uranyl and the latter was attributed to uranium atom binding with the oxygen atom in manganese dioxide.

The C 1s signals (shown in **Figure 7(d)**) was deconvoluted into three peaks at 288.52 eV, 285.65 eV and 284.53 eV assigned to carbon in C=O, C-O and C-C bonds, in which the former chemical bonds slightly shifted to 288.57 eV and 285.71 eV owing to the participation of oxygen in interaction with uranium.

The Mn 2p signal shown in **Figure 7(c)** presented as Mn $2p_{1/2}$ and Mn $2p_{3/2}$ corresponding to the Mn-O bond. The slight change in binding energy proved that manganese did not directly interact with uranium.

Obvious distinct are observed in the spectrum of O 1s (shown in **Figure 7(b)**). Indetail, the O 1s signal was splitted into four peaks originally positioned at 532.89 eV, 531.73 eV, 531.27 eV and 529.39 eV assigned as C-O, C=O, Mn-O-H and Mn-O-Mn. After adsorption, the binding energy changed obviously and the relative intensity of four peaks varied significantly. The obvious distinct proved oxygen atom was the major donor atom. The adsorption mechanism of uranium onto MnO_2-PVA/PAA is thus proposed as **Figure 7(f)**. Namely the fixed uranyl

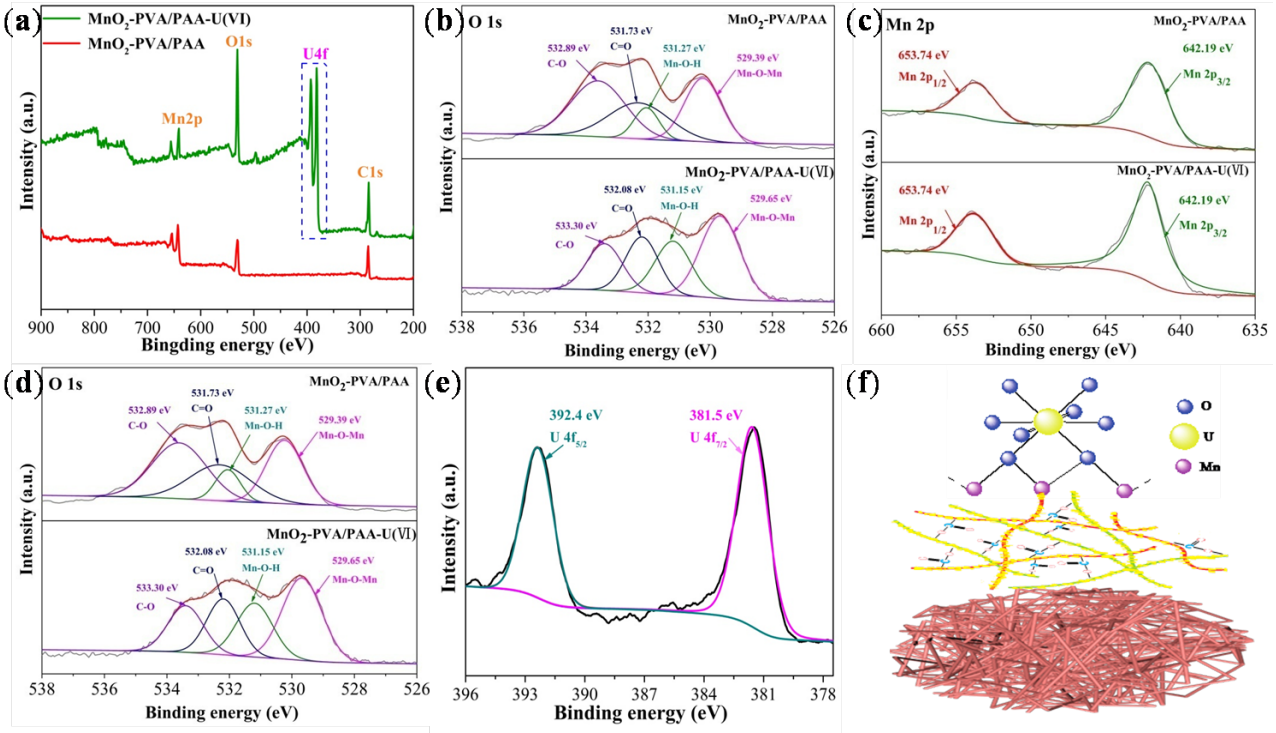

Figure 7. XPS spectra (a) full spectrum, (b) O 1s, (c) Mn 2P, (d) C 1s, and (e) U 4f of MnO_2-PVA/PAA and MnO_2-PVA/PAA-U(VI); (f) The proposal mechanism of uranium interacting with MnO_2-PVA/PAA.

with MnO_2-PVA/PAA was anchored with two oxygen atoms in manganese dioxide.

4. Conclusion

In the study a novel manganese dioxide modified nanofiber, MnO_2-PVA/PAA, was facile prepared using the electrospinning technique. MnO_2-PVA/PAA was proved by SEM, FT-IR, XRD, stress-strain test. Effect of pH, ionic strength, initial uranium concentration, mixing time, temperature on the adsorption, reusability and adsorption mechanism were illustrated. The optimal pH was determined as 6.0. The adsorption took the way of inner-sphere surface complex. The theoretical adsorption amount of MnO_2-PVA/PAA calculated as 398.85 mg/g. The pseudo-second-order kinetics well fitted the adsorption process, illustrating chemical mode. The thermodynamic parameter ΔH° and ΔS° were 13.55 kJ·mol^{-1} and 106.04 J·K^{-1}·mol^{-1}. The absolute value of ΔG° increased as the temperature increased. XPS revealed that uranyl complexed MnO_2-PVA/PAA through the U-O-Mn bond. The results herein demonstrated high potential of MnO_2-PVA/PAA as a candidate in separation for uranium.

Acknowledgements

This work was financially supported by the National Natural Science Foundation of China (22066001).

Conflicts of Interest

The authors declare no conflicts of interest regarding the publication of this paper.

References

[1] Abas, N., Kalair, A. and Khan, N.J.F. (2015) Review of Fossil Fuels and Future Energy Technologies. *Futures*, **69**, 31-49. https://doi.org/10.1016/j.futures.2015.03.003

[2] Hore-Lacy, I. (2016) Uranium for Nuclear Power: An Introduction, Uranium for Nuclear Power. 1st Edition, Woodhead Publishing Ltd., Cambridge, 3-10. https://doi.org/10.1016/B978-0-08-100307-7.00001-6

[3] Tao, Q.Q., Zhang, X., Prabaharan, K. and Dai, Y. (2019) Separation of Cesium from Wastewater with Copper Hexacyanoferrate Film in an Electrochemical System Driven by Microbial Fuel Cells. *Bioresour. Technol.*, **278**, 456-459. https://doi.org/10.1016/j.biortech.2019.01.093

[4] Ma, F., Gui, Y., Liu, P., Xue, Y. and Song, W. (2020) Functional Fibrous Materials-Based Adsorbents for Uranium Adsorption and Environmental Remediation. *Chem. Eng. J.*, **390**, 124597. https://doi.org/10.1016/j.cej.2020.124597

[5] Singh, D., Hareendran, K., Sreenivas, T., Kain, V. and Dey, G. (2017) Development of a Phosphate Precipitation Method for the Recovery of Uranium from Lean Tenor Alkaline Leach Liquor. *Hydrometallurgy*, **171**, 228-235. https://doi.org/10.1016/j.hydromet.2017.05.021

[6] Prabhu, D.R., Mohapatra, P.K., Raut, D.R., Pathak, P. and Billard, I. (2017) Extraction of Uranium (VI) from Nitric Acid Solutions Using N, N-Dihexyloctanamide in Ionic Liquids: Solvent Extraction and Spectroscopic Studies. *Solvent Extr. Ion Exch.* **35**, 423-438. https://doi.org/10.1080/07366299.2017.1377423

[7] Amphlett, J.T.M., Choi, S., Parry, S.A., Moon, E.M., Sharrad, C.A. and Ogden, M.D. (2019) Insights on Uranium Uptake Mechanisms by Ion Exchange Resins with Chelating Functionalities: Chelation vs. Anion Exchange. *Chem. Eng. J.*, **392**, 123712. https://doi.org/10.1016/j.cej.2019.123712

[8] Jung, Y., Kim, S., Park, S.J. and Kim, J.M. (2008) Application of Polymer-Modified Nanoporous Silica to Adsorbents of Uranyl Ions. *Colloid Surf. A*: *Physicochem. Eng. Asp.*, **313**, 162-166. https://doi.org/10.1016/j.colsurfa.2007.04.087

[9] Bessbousse, H., Rhlalou, T., Verchère, J.F. and Lebrun, L. (2008) Removal of Heavy Metal Ions from Aqueous Solutions by Filtration with a Novel Complexing Membrane Containing Poly (Ethyleneimine) in a Poly (Vinyl Alcohol) Matrix. *J. Membr. Sci.*, **307**, 249-259. https://doi.org/10.1016/j.memsci.2007.09.027

[10] Liang, P.L., Yuan, L.Y., Deng, H., Wang, X.C., Wang, L., Li, Z.J., Luo, S.Z. and Shi, W.Q. (2020) Photocatalytic Reduction of Uranium (VI) by Magnetic $ZnFe_2O_4$ under Visible Light. *Applied Catalysis B*: *Environmenta*, **267**, 118688. https://doi.org/10.1016/j.apcatb.2020.118688

[11] Li, F.F., Cui, W.R., Jiang, W., Zhang, C.R., Liang, R.P. and Qiu, J.D. (2020) Stable sp^2 Carbon-Conjugated Covalent Organic Framework for Detection and Efficient Adsorption of Uranium from Radioactive Wastewater. *J. Hazard. Mater.*, **392**, 122333. https://doi.org/10.1016/j.jhazmat.2020.122333

[12] Drysdale, J.A. and Buesseler, K.O. (2020) Uranium Adsorption Behaviour of Amidoximated Fibers under Coastal Ocean Conditions. *Prog. Nucl. Energy*, **119**, 103170. https://doi.org/10.1016/j.pnucene.2019.103170

[13] Pan, N., Li, L., Ding, J., Li, S., Wang, R., Jin, Y., Wang, X. and Xia, C. (2016) Preparation of Graphene Oxide-Manganese Dioxide for Highly Efficient Adsorption and Separation of Th(IV)/U(VI). *J. Hazard. Mater.*, **309**, 107-115. https://doi.org/10.1016/j.jhazmat.2016.02.012

[14] Yang, C., Zhong, Y., Li, L., Ren, X., Sun, Y., Niu, D., Liu, Y., Yin, M. and Zhang, D. (2018) Lead and Uranium Sorption Characteristics on Hydrothermal Synthesized Delta Manganese Dioxide. *J. Radioanal. Nucl. Chem.*, **317**, 1399-1408. https://doi.org/10.1007/s10967-018-6004-0

[15] Zhu, Q. and Li, Z. (2015) Hydrogel-Supported Nanosized Hydrous Manganese Dioxide: Synthesis, Characterization, and Adsorption Behavior Study for Pb^{2+}, Cu^{2+}, Cd^{2+} and Ni^{2+} Removal from Water. *Chem. Eng. J.*, **281**, 69-80. https://doi.org/10.1016/j.cej.2015.06.068

[16] Kim, E.J., Lee, C.-S., Chang, Y.-Y. and Chang, Y.-S. (2013) Hierarchically Structured Manganese Oxide-Coated Magnetic Nanocomposites for the Efficient Removal of Heavy Metal Ions from Aqueous Systems. *ACS Appl. Mater. Interfaces*, **5**, 9628-9634. https://doi.org/10.1021/am402615m

[17] Xue, J., Wu, T., Dai, Y. and Xia, Y. (2019) Electrospinning and Electrospun Nanofibers: Methods, Materials, and Applications. *Chem. Rev.*, **119**, 5298-5415. https://doi.org/10.1021/acs.chemrev.8b00593

[18] Sun, W., Lu, X., Tong, Y., Lei, J., Nie, G. and Wang, C. (2014) A One-Pot Synthesis of a Highly Dispersed Palladium/Polypyrrole/Polyacrylonitrile Nanofiber Membrane and Its Recyclable Catalysis in Hydrogen Generation from Ammonia Borane. *J. Mater. Chem. A*, **2**, 6740-6746. https://doi.org/10.1039/C3TA15441F

[19] Li, Y., Lee, D.K., Kim, J.Y., Kim, B., Park, N.G., Kim, K., Shin, J.H., Choi, I.S. and Ko, M.J. (2012) Highly Durable and Flexible Dye-Sensitized Solar Cells Fabricated On Plastic Substrates: PVDF-Nanofiber-Reinforced TiO_2 Photoelectrodes. *Energy Environ. Sci.*, **5**, 8950-8957. https://doi.org/10.1039/c2ee21674d

[20] Gu, X., Ding, F. and Williams, D.F. (2014) Neural Tissue Engineering Options for Peripheral Nerve Regeneration. *Biomaterials*, **35**, 6143-6156. https://doi.org/10.1016/j.biomaterials.2014.04.064

[21] Selvam, A.K. and Nallathambi, G. (2015) Polyacrylonitrile/Silver Nanoparticle Electrospun Nanocomposite Matrix for Bacterial Filtration. *Fiber. Polym.*, **16**, 1327-1335. https://doi.org/10.1007/s12221-015-1327-8

[22] Xie, J.H., Lv, R.W., Peng, H., Fan, J.L., Tao, Q.Q., Dai, Y., Zhang, Z., Cao, X. and Liu, Y.H. (2020) Phosphate Functionalized Poly(Vinyl Alcohol)/Poly(Acrylic Acid) (PVA/PAA): An Electrospinning Nanofiber for Uranium Separation. *J. Radioanal. Nucl. Chem.*, **326**, 475-486. https://doi.org/10.1007/s10967-020-07319-x

[23] Dastbaz, A. and Keshtkar, A.R. (2014) Adsorption of Th^{4+}, U^{6+}, Cd^{2+}, and Ni^{2+} from Aqueous Solution by a Novel Modified Polyacrylonitrile Composite Nanofiber Adsorbent Prepared by Electrospinning. *Appl. Surf. Sci.*, **293**, 336-344. https://doi.org/10.1016/j.apsusc.2013.12.164

[24] Yari, S., Abbasizadeh, S., Mousavi, S.E., Moghaddam, M.S. and Moghaddam, A.Z. (2015) Adsorption of Pb (II) and Cu (II) Ions from Aqueous Solution by an Electrospun CeO_2 Nanofiber Adsorbent Functionalized with Mercapto Groups. *Process Saf. Environ. Protect.*, **94**, 159-171. https://doi.org/10.1016/j.psep.2015.01.011

[25] Irani, M., Keshtkar, A.R. and Moosavian, M.A. (2012) Removal of Cadmium from Aqueous Solution Using Mesoporous PVA/TEOS/APTES Composite Nanofiber Prepared by Sol-Gel/Electrospinning. *Chem. Eng. J.*, **200**, 192-201. https://doi.org/10.1016/j.cej.2012.06.054

[26] Alipour, D., Keshtkar, A.R. and Moosavian, M.A. (2016) Adsorption of Thorium (IV) from Simulated Radioactive Solutions Using a Novel Electrospun PVA/TiO_2/ZnO Nanofiber Adsorbent Functionalized with Mercapto Groups: Study in Single and Multi-Component Systems. *Appl. Surf. Sci.*, **366**, 19-29. https://doi.org/10.1016/j.apsusc.2016.01.049

[27] Mahapatra, A., Mishra, B. and Hota, G. (2013) Electrospun Fe_2O_3-Al_2O_3 Nanocomposite Fibers as Efficient Adsorbent for Removal of Heavy Metal Ions from Aqueous Solution. *J. Hazard. Mater.*, **258**, 116-123. https://doi.org/10.1016/j.jhazmat.2013.04.045

[28] Abbasizadeh, S., Keshtkar, A.R. and Mousavian, M.A. (2013) Preparation of A Novel Electrospun Polyvinyl Alcohol/Titanium Oxide Nanofiber Adsorbent Modified with Mercapto Groups for Uranium (VI) and Thorium (IV) Removal from Aqueous Solution. *Chem. Eng. J.*, **220**, 161-171. https://doi.org/10.1016/j.cej.2013.01.029

[29] Beheshti, H., Irani, M., Hosseini, L., Rahimi, A. and Aliabadi, M. (2016) Removal of Cr (VI) from Aqueous Solutions Using Chitosan/MWCNT/Fe_3O_4 Composite Nanofibers-Batch and Column Studies. *Chem. Eng. J.*, **284**, 557-564. https://doi.org/10.1016/j.cej.2015.08.158

[30] Aliabadi, M., Irani, M., Ismaeili, J. and Najafzadeh, S. (2014) Design and Evaluation of Chitosan/Hydroxyapatite Composite Nanofiber Membrane for the Removal of Heavy Metal Ions from Aqueous solution. *J. Taiwan Inst. Chem. Eng.*, **45**, 518-526. https://doi.org/10.1016/j.jtice.2013.04.016

[31] Zong, P., Wu, X., Gou, J., Lei, X., Liu, D. and Deng, H. (2015) Immobilization and Recovery of Uranium (VI) Using Na-Bentonite from Aqueous Medium: Equilibrium, Kinetics and Thermodynamics Studies. *J. Mol. Liq.*, **209**, 358-366.

https://doi.org/10.1016/j.molliq.2015.05.052

[32] Zhang, J., Guo, Z., Li, Y., Pan, S., Chen, X. and Xu, J. (2016) Effect of Environmental Conditions on the Sorption of Uranium on Fe_3O_4@MnO_2 Hollow Spheres. *J. Mol. Liq.*, **223**, 534-540. https://doi.org/10.1016/j.molliq.2016.07.136

[33] Yang, C., Niu, D., Zhong, Y., Li, L., Lv, H. and Liu, Y. (2018) Adsorption of Uranium by Hydrous Manganese Dioxide from Aqueous Solution. *J. Radioanal. Nucl. Chem.*, **315**, 533-542. https://doi.org/10.1007/s10967-018-5705-8

[34] Wang, X., Zhu, G. and Guo, F. (2013) Removal of Uranium (VI) Ion from Aqueous Solution by SBA-15. *Ann. Nucl. Energy*, **56**, 151-157. https://doi.org/10.1016/j.anucene.2013.01.041

[35] Yang, S., Qian, J., Kuang, L. and Hua, D. (2017) Ion-Imprinted Mesoporous Silica for Selective Removal of Uranium from Highly Acidic and Radioactive Effluent. *ACS Appl. Mater. Interfaces*, **9**, 29337-29344. https://doi.org/10.1021/acsami.7b09419

[36] Sun, Y., Wu, Z.-Y., Wang, X., Ding, C., Cheng, W., Yu, S.-H. and Wang, X. (2016) Macroscopic and Microscopic Investigation of U (VI) and Eu (III) Adsorption on Carbonaceous Nanofibers. *Environ. Sci. Technol.*, **50**, 4459-4467. https://doi.org/10.1021/acs.est.6b00058

[37] Monier, M. and Elsayed, N.H. (2014) Selective Extraction of Uranyl Ions Using Ion-Imprinted Chelating Microspheres. *J. Colloid Interface Sci.*, **423**, 113-122. https://doi.org/10.1016/j.jcis.2014.02.015

[38] Zhang, J., Zhang, H., Liu, Q., Song, D., Li, R., Liu, P. and Wang, J. (2019) Diaminomaleonitrile Functionalized Double-Shelled Hollow MIL-101 (Cr) for Selective Removal of Uranium from Simulated Seawater. *Chem. Eng. J.*, **368**, 951-958. https://doi.org/10.1016/j.cej.2019.02.096

[39] Hamza, M.F., Aly, M.M., Abdel-Rahman, A.A.-H., Ramadan, S., Raslan, H., Wang, S., Vincent, T. and Guibal, E. (2017) Functionalization of Magnetic Chitosan Particles for the Sorption of U (VI), Cu (II) and Zn (II): Hydrazide Derivative of Glycine-Grafted Chitosan. *Materials*, **10**, 539. https://doi.org/10.3390/ma10050539

[40] Christou, C., Philippou, K., Krasia-Christoforou, T. and Pashalidis, I. (2019) Uranium Adsorption by Polyvinylpyrrolidone/Chitosan Blended Nanofibers. *Carbohydr. Polym.*, **219**, 298-305. https://doi.org/10.1016/j.carbpol.2019.05.041

[41] Saleh, T.A., Tuzen, M. and Sarı, A. (2017) Polyethylenimine Modified Activated Carbon as Novel Magnetic Adsorbent for the Removal of Uranium from Aqueous Solution. *Chem. Eng. Res. Des.*, **117**, 218-227. https://doi.org/10.1016/j.cherd.2016.10.030

[42] Li, M., Liu, H., Chen, T., Dong, C. and Sun, Y. (2019) Synthesis of Magnetic Biochar Composites for Enhanced Uranium (VI) Adsorption. *Sci. Total Environ.*, **651**, 1020-1028. https://doi.org/10.1016/j.scitotenv.2018.09.259

[43] Abdi, S., Nasiri, M., Mesbahi, A. and Khani, M.H. (2017) Investigation of Uranium (VI) Adsorption by Polypyrrole. *J. Hazard. Mater.*, **332**, 132-139. https://doi.org/10.1016/j.jhazmat.2017.01.013

[44] Anirudhan, T.S., Lekshmi, G.S. and Shainy, F. (2019) Synthesis and Characterization of Amidoxime Modified Chitosan/Bentonite Composite for the Adsorptive Removal and Recovery of Uranium from Seawater. *J. Colloid Interface Sci.*, **534**, 248-261. https://doi.org/10.1016/j.jcis.2018.09.009

[45] Xie, L., Zhong, Y., Xiang, R., Fu, G., Xu, Y., Cheng, Y., Liu, Z., Wen, T., Zhao, Y.

and Liu, X. (2017) Sono-Assisted Preparation of Fe (II)-Al (III) Layered Double Hydroxides and Their Application for Removing Uranium (VI). *Chem. Eng. J.*, **328**, 574-584. https://doi.org/10.1016/j.cej.2017.07.051